THE JOURNAL OF PHYSICAL CHEMISTRY A

Article

pubs.acs.org/JPCA

Measurements of Thermodynamic and Optical Properties of Selected Aqueous Organic and Organic–Inorganic Mixtures of Atmospheric Relevance

Daniel M. Lienhard,*[,†,‡] David L. Bones,[‡] Andreas Zuend,[¶] Ulrich K. Krieger,[†] Jonathan P. Reid,[‡] and Thomas Peter[†]

[†]Institute for Atmospheric and Climate Science, ETH Zürich, Zürich, Switzerland

[‡]School of Chemistry, University of Bristol, Bristol BS8 1TS, United Kingdom

[¶]Department of Chemical Engineering, California Institute of Technology, Pasadena, California, United States

ABSTRACT: Atmospheric aerosol particles can exhibit liquid solution concentrations supersaturated with respect to the dissolved organic and inorganic species and supercooled with respect to ice. In this study, thermodynamic and optical properties of sub- and supersaturated aqueous solutions of atmospheric interest are presented. The density, refractive index, water activity, ice melting temperatures, and homogeneous ice freezing temperatures of binary aqueous solutions containing L(+)-tartaric acid, tannic acid, and levoglucosan and ternary aqueous solutions containing levoglucosan and one of the salts NH_4HSO_4, $(NH_4)_2SO_4$, and NH_4NO_3 have been measured in the supersaturated concentration range for the first time. In addition, the density and refractive index of binary aqueous citric acid and raffinose solutions and the glass transition temperatures of binary aqueous L(+)-tartaric acid and levoglucosan solutions have been measured. The data presented here are derived from experiments on single levitated microdroplets and bulk solutions and should find application in thermodynamic and atmospheric aerosol models as well as in food science applications.

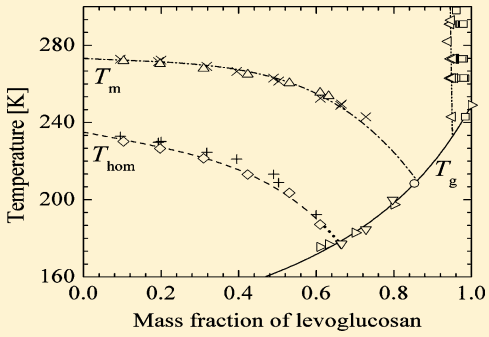

INTRODUCTION

Atmospheric aerosol particles significantly affect the Earth's radiation budget and atmospheric chemistry by scattering and absorbing light or providing surfaces for heterogeneous chemistry. Both processes hinge on the size, phase, and chemical composition of these particles.[1] It is therefore crucial to improve our current understanding of the thermodynamic and optical properties of the substances commonly found in atmospheric particles at tropospheric humidities and temperatures. Aged atmospheric particles consist of a number of inorganic and a myriad of organic substances,[2,3] many of which are unidentified on the molecular level. The hygroscopic behavior of aerosols has therefore been studied using model substances or model mixtures representing substance classes typically found in aerosol particles.[4−6] While the inorganic part has been well-characterized from dilute to supersaturated conditions, data for specific organic and mixed organic as well as inorganic–organic mixtures are scarce compared to the large number of organic compounds that have been identified in atmospheric particles.

The selection of mixtures investigated in this study is designed to fill gaps in the understanding of the interaction between water as the solvent and an organic solute as well as of the interactions in ternary systems containing salts. Thus, the data presented may be applied to verify and/or parametrize thermodynamic models that allow predictions for activities in mixtures as complex as atmospheric aerosol.[7] In addition, parametrizations for the aqueous solutions are needed to interpret microphysical experiments, for example, on cirrus cloud formation.[8]

Levoglucosan (1,6-anhydro-β-D-glucopyranose), a product of pyrolysis of sugar derivatives,[9−12] has been identified as the single most abundant component in aerosol particles near biomass burning sites[13−15] and is used as a tracer for cellulose and atmospheric particles.[16] Nevertheless, because thermodynamic data of levoglucosan are scarce,[6,17,18] this substance is investigated in detail in this study.

Citric acid and L(+)-tartaric acid were chosen because they have been identified in aerosol particles[15,19,20] and have been frequently used as model substances for atmospheric experiments.[21,22] Both compounds are also of interest in food and pharmaceutical sciences.[23−25] Raffinose and tannic acid can be regarded as proxies for oxidized organic molecules with high molar masses.

Ternary aqueous solutions containing levoglucosan and ammonium bisulfate (NH_4HSO_4), ammonium sulfate [$(NH_4)_2SO_4$], and ammonium nitrate (NH_4NO_3) with a 1:1 molar ratio of the organic and the salt are investigated in this

Received: June 7, 2012
Revised: August 10, 2012
Published: September 13, 2012

paper to study the interaction between levoglucosan and salts with known thermodynamic and optical properties[26−28] that are commonly found in atmospheric particles.[29]

In this work, we present measurements of the dependence of water activity (a_w), density (ρ), refractive index (n), ice melting temperature (T_m), homogeneous ice freezing temperatures (T_{hom}), and glass transition temperature (T_g) on the mass fraction of the solute (mfs) or molarity of the solute (M). These measurements are compared to predictions from the AIOMFAC model,[7,30] the UNIFAC model,[31,32] the Zdanovskii−Stokes−Robinson (ZSR) relation[33−35] and mixing rules of the molar volumes and refractivities to investigate the accuracy of these models and mixing rules. In this study, "solute" refers to the inorganic and/or organic components in the aqueous solution, with water defined as the solvent. Hence, mfs refers to the summed mass of the water-free components relative to the mass of the overall water-containing solution. The parametrizations of the above-mentioned properties are presented in Tables 1 and 2 in a form such that they can directly be included in thermodynamic and atmospheric aerosol models.

METHODS

Thermodynamic properties of aqueous solutions were investigated in optical tweezers and in an electrodynamic balance (EDB) with varying relative humidity (RH) and temperature. Note that in this paper, water activity refers to the property of the liquid phase, while RH refers to the gas phase. Phase transitions have been observed in a differential scanning calorimeter (DSC). These three techniques are described in detail elsewhere[36−41] and are only briefly summarized below.

Bulk a_w measurements, solution refractometry, and pycnometry were carried out at 298 K in an AquaLab dewpoint hygrometer (Model 3TE, Decagon devices, U.S.A., uncertainty ±0.003), a Zeiss Abbe refractometer [589 nm (sodium D-line), uncertainty ±0.0002], and a Blaubrand pycnometer (10 cm^3 nominal volume, uncertainty ±0.0015 g cm^{-3}), respectively.

The solutions were made with deionized water (resistivity ≥ 18.2 M Ω cm). All substances were used without further purification: raffinose (Sigma, 98%), tannic acid (Sigma, 99.5%, CAS No. 1401-55-4), L(+)-tartaric acid (Sigma, 99.5%), levoglucosan (ABCR, 99%), citric acid (Sigma, 99%), NH_4HSO_4 (Aldrich, 99.999%), $(NH_4)_2SO_4$ (Fluka, 99.5%), and NH_4NO_3 (Fluka, 99.5%). The estimated error in the solution preparation is ±0.005 in mass fraction.

Optical Tweezers. The optical tweezers used in this study consisted of a Nd:YVO_4 laser (frequency-doubled, 532 nm) that was tightly focused to form a single-beam gradient force optical trap by an inverted microscope configuration with an oil immersion microscope objective (numerical aperture of 1.25, 100× magnification). The trap was loaded by an aerosol mist generated by a medical nebulizer. When a particle approached the laser focus, its induced dipole interacted with the electromagnetic field of the laser, trapping the particle in the focus of the beam. The flows of dry and humidified nitrogen gas were controlled via mass flow meters and needle valves, allowing the RH to be varied. The temperature was maintained at around 298 K, and the uncertainty in the RH was 2%. The whispering gallery modes (WGMs' see Figure 1) occurring in the backscattered stimulated Raman signatures from OH and CH stretching vibrations (between 620 and 665 nm with 532 nm illumination) could be assigned either transverse electric (TE_l^n) or transverse magnetic (TM_l^n) polarization, where n denotes the mode number and l the mode order. Raman

Table 1. Parameters for T_m, T_{hom}, ρ, and n According to Equations 1, 2, 7, and 8[a]

solutes	T_m [K]			T_{hom} [K]			ρ [g cm^{-3}]			n			
	m_1	m_2	mfs range	h_1	h_2	mfs range	d_1	d_2	V [cm^3 mol^{-1}]	n_1	n_2	R [cm^3 mol^{-1}]	ρ_c [g cm^{-3}]
raffinose[b]	−6.63153	−52.28235	mfs < 0.800	−18.86872	−167.86953	mfs < 0.514	0.41755	0.09769	333.6	0.07597	−0.00162	105.7	1.815[f]
citric acid[c]							0.38804	0.19537	121.6	0.02383	−0.0003	36.27	1.665[g]
L(+)-tartaric acid	−15.3198	−177.62452	mfs < 0.738	−43.59914	−338.20337	mfs < 0.410	0.41014	0.25729	90.17	0.01842	−0.00029	26.59	1.759[h]
tannic acid[d]	−0.14204	−9.17458	mfs < 0.703				0.43099	0.13365	1089.3	0.3421		395.9	2.129[f]
levoglucosan	−7.89834	−103.48546	mfs < 0.853	−38.04688	−169.80495	mfs < 0.610	0.36893	0.1461	107.2	0.02162	−0.00007	33.04	1.618[i]
levoglucosan/NH_4HSO_4[e]	−24.79179	−96.65633	mfs < 0.548	−46.91731	−369.90974	mfs < 0.548	0.462[e]	0.24683[e]	162.5 (174.8[m])	0.01653	−0.00022	48.0 (51.7[k])	1.685[j]
levoglucosan/$(NH_4)_2SO_4$	−24.91448	−101.2942	mfs < 0.497	−50.79146	−195.32767	mfs < 0.497	0.39526	0.25378	178.8 (196.8[m])	0.02055	−0.00039	53.8 (56.8[k])	1.686[j]
levoglucosan/NH_4NO_3	−24.06235	−40.86483	mfs < 0.803	−41.964	−77.79736	mfs < 0.702	0.3539	0.17317	158.9 (159.6[m])	0.01568	−0.00009	48.0 (50.1[l])	1.652[j]

[a]The mfs ranges for T_m and T_{hom} describe the concentration ranges where measurements are available. The molar volumes V and molar refractivities R (eq 12) are calculated based on the densities and refractive indices of the pure solutes, treating the two different solute molecules in the ternary systems as one molecule with the combined molar weight. The values in brackets denote the sum of the V and R of the two individual solute compounds. The densities of the crystal of the solutes at 298 K (ρ_c) are listed in the last column. For the ternary systems, ρ_c is calculated using the crystal densities of the individual solutes weighted by their molar mass. [b]T_m and T_{hom} fit curves are based on data reported by refs 37. 103, and 104. [c]T_m and T_{hom} fit curves can be found in ref 105. [d]The high viscosity of aqueous tannic acid solutions prevented the use of emulsified samples and thus the determination of T_{hom}. [e]For aqueous levoglucosan/NH_4HSO_4 solutions, the parametrization of the density is $\rho = 0.9971 + d_1$·mfs $+ d_2$·mfs^3. [f]Predicted using ACD/PhysChem Suite [Advanced Chemistry Development, Inc. (http://www.acdlabs.com)]. [g]From ref 84. [h]From ref 84, assuming that L(+)-tartaric acid exhibits the same crystal density as D-tartaric acid. [i]From ref 106. [j]Calculated based on the crystal densities of levoglucosan from ref 106 and the salts from refs 86 and 87. [k]Molar refractivity of the salts taken from ref 27. [l]Molar refractivity of NH_4NO_3 calculated from the refractive index reported by ref 28 and the molar volume reported by refs 86 and 87. [m]Calculated applying the molar volumes reported by refs 86 and 87.

dx.doi.org/10.1021/jp3055872 | J. Phys. Chem. A 2012, 116, 9954−9968

Table 2. Fit Parameters for the a_w Parameterization According to Equation 4[a]

solute	a_1	a_2	a_3	a_4	a_5	a_6	T range	mfs range
citric acid[b]	−3.16761	0.01939	-4.02725×10^{-5}	6.59108	−0.05294	1.06028×10^{-4}	220< T < 298	mfs < 0.750
L(+)-tartaric acid[c]	−0.70237	-8.28222×10^{-4}		0.08066	5.85333×10^{-4}		205< T < 298	mfs < 0.740
levoglucosan[d,e]	1.1888	−0.01305	1.93905×10^{-5}	−1.8548	0.01026	-1.18649×10^{-5}	243< T < 313	
	−1.75974	0.00379		1.21029	−0.00523		185< T < 243	
levoglucosan/NH_4HSO_4	−0.64459	-8.95976×10^{-4}		−0.04052	6.34437×10^{-4}		170< T < 298	mfs < 0.548
levoglucosan/$(NH_4)_2SO_4$[e]	−0.45741	−0.0016		−0.64624	0.00304		190< T < 298	mfs < 0.497
levoglucosan/NH_4NO_3	−0.60817	-8.59444×10^{-4}		−0.66162	0.00243		180< T < 298	mfs < 0.702

[a]The range of validity with respect to temperature is indicated. The range of validity with respect to mfs for temperatures lower than 290.6 K is indicated in the last column. For levoglucosan, the temperature range has been split into two temperature ranges and is valid for all concentrations. All T_m and T_{hom} values experimentally determined in this study (Table 3 in the Appendix) and found in the literature for each specific solute have been used to find the temperature dependence of a_w. Raffinose has been investigated in a previous study[37] and is not listed here. The data for tannic acid only covers a very small range of water activities from 0.995 (at mfs = 0.703, corresponding to a mole fraction of 0.024) to 1 and were not parametrized. [b]Includes a_w measurements from refs 4, 5, 94, and 107−109. [c]Includes a_w measurements from refs 4, 107-109. [d]Includes a_w measurements from refs 6 and 18. [e]The parametrization shows good agreement with T_m and T_{hom} measurements from refs 110 and 111, which used a different technique.

spectra were taken with a time resolution of 2 s.[42] The radii and refractive indices of optically trapped droplets ranged from 2.5 to 5 μm and from 1.38 to 1.52, respectively, which led to the appearance of first- and second-order modes. An example is shown in Figure 1 for a droplet containing levoglucosan and NH_4NO_3 (1:1 molar ratio) equilibrated at 6% RH at 298 K. The wavelengths of the WGM are compared to predictions from Mie scattering theory to find the size and refractive index of the trapped particle simultaneously and assign the polarization, mode number, and mode order of each resonance.[26,43,44] The uncertainty in the refractive index and radius extraction are estimated to be 0.0025 and 5 nm, respectively. It is assumed that the refractive index dispersion depends linearly on the wavelength, as shown in Figure 1a. The refractive index parametrizations listed in Table 1 and the measurements shown in Figure 4 refer to a wavelength of 589 nm. All values and uncertainties reported here are derived from particles that are fully equilibrated to the RH and temperature in the chamber. Highly viscous particles such as the ones containing citric acid or raffinose at very low RH require very long equilibration times and were not measured in this work.

Electrodynamic Balance. The EDB consists of a double ring balance in a three-wall glass chamber with a cooling liquid flowing through the inner walls and an insulation vacuum between the outer walls. A single-particle generator (Hewlett−Packard 51633A ink jet cartridge) is used to inject a charged particle, which is levitated by the electric fields generated by two ring electrodes (AC field) and two end-cap electrodes (DC field). The dc voltage tracks the mass change of the particle and thus measures its water activity as a function of mfs when the particle is in equilibrium with the RH of the gas phase, and no evaporation of the solute occurs. The RH in the EDB is controlled in the same way as that in the optical tweezers, while the temperature can be varied between 190 and 310 K with stability better than 0.1 K and accuracy of ±0.5 K. However, the experiments are carried out below 291 K to keep the dew point temperature of the mixed flow always below the temperature of the lab (293 K). The levitated particle is illuminated by a HeNe laser and an LED that emits light between 560 and 610 nm with high spatial coherence. The two-dimensional angular scattering pattern is recorded with a CCD sensor that measures the elastically scattered light from the HeNe laser at a 633 nm wavelength between observation angles of 78 and 101°. A spherical particle will show a regular scattering pattern, while a nonspherical particle shows an irregular scattering pattern.[45,46] The backscattered light from the LED is collected by a spectrograph with a slow scan back-illuminated CCD array detector as an optical multichannel analyzer with a resolution of 0.2 nm. Here, the integration time was 10 s, and the elapsed time between two spectra was between 30 and 120 s. The changes in the wavelengths of the Mie resonances in the spectra are used to calculate the particle radius and thus the solute concentration when the refractive index and the density are known.[38] The concentration derived from LED measurements can be compared to the mass measurement to provide additional data for the parametrizations of n and ρ summarized in Table 1.

Differential Scanning Calorimetry. T_m, T_{hom}, and T_g of different concentrated aqueous solutions were investigated in a DSC (TA Instruments Q10). Melting and freezing temperatures were measured with a heating rate of 1 K min^{-1} and a cooling rate of 10 K min^{-1}. Glass transition temperatures were determined as the onset point of the heat signal in the heating cycle with a heating rate of 10 K min^{-1} in bulk samples or emulsified samples to avoid crystallization on the surface of the pan holding the sample.[37,47] Emulsions were prepared by adding four parts by mass of a mixture with a lanolin (Fluka Chemical) mass fraction of 0.23 and a mineral oil (Aldrich Chemical) mass fraction of 0.77 to one part of the solution of interest.[36] Stirring with a rotor-stator homogenizer (Polytron PT 1300 D with a PT-DA 1307/2EC dispersing aggregate) for 40 s at 7000 rpm led to droplets with diameters in the range of 0.5−5 μm.[48] The uncertainty in absolute temperature was ±1.2 K for T_{hom}, ±0.8 K for T_m, and ±0.9 K for T_g.

RESULTS

Phase Transitions. All phase transitions measured in this study are listed in Table 3 in the Appendix. For T_m and T_{hom}, the following parametrizations were chosen

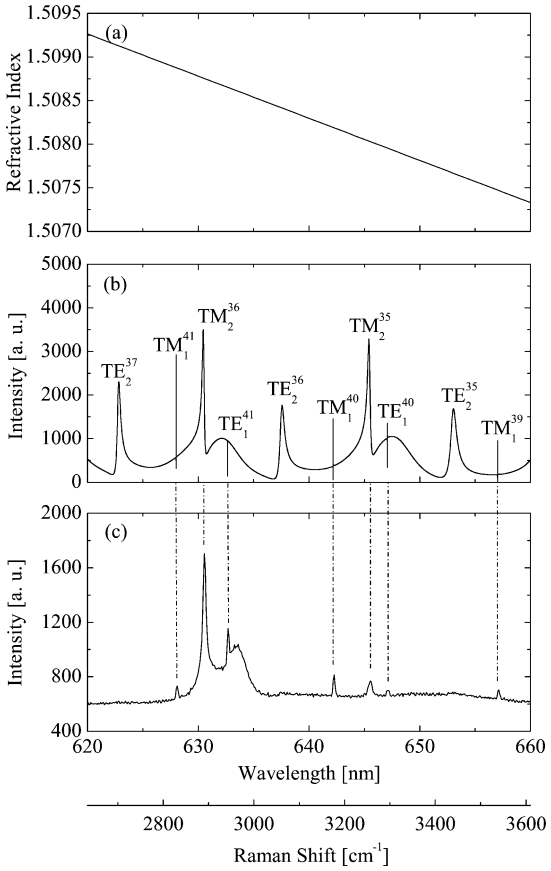

Figure 1. Refractive index (a), computed elastic backscattered intensity (b), and observed backscattered intensity (c) of an optically tweezed particle in the range of the CH and OH stretching vibrations as a function of wavelength or Raman shift at 532 nm illumination. While the positions of the measured and calculated resonant wavelengths are in agreement, the intensities do not match because of nonlinear effects in the Raman scatter. This spectrum is from a particle of radius 3097 nm, containing levoglucosan and NH_4NO_3 with a 1:1 molar ratio equilibrated at 6% RH at 298 K. The observed spectrum shows WGMs that are assigned to five first- and two second-order modes in the computed spectrum (see dashed–dotted lines). The intensities of the modes TE_2^{37}, TE_2^{36}, and TE_2^{35} were too weak to be detected in the stimulated Raman fingerprint of the CH and OH stretching vibrations.

$$T_m = 273.15 + m_1 \cdot \mathrm{mfs} + m_2 \cdot \mathrm{mfs}^4 \quad (1)$$

$$T_{hom} = 235 + h_1 \cdot \mathrm{mfs} + h_2 \cdot \mathrm{mfs}^4 \quad (2)$$

The corresponding values of the parameters m_1, m_2, h_1, and h_2 can be found in Table 1. The phase diagrams of levoglucosan and L(+)-tartaric acid are shown in Figure 2. T_g' denotes the glass transition temperature of the freeze-concentrated solution that is accessible in DSC scans.[49] The T_g' value of 208.4 K for levoglucosan measured in this study is in good agreement with values found in the literature.[50] Kadoya et al.[51] and Izutsu et al.[52] found the midpoint of the heat signal of T_g' of L(+)-tartaric acid at 216.1 K, in good agreement with the onset point of 208.5 K found in this study. Note that Figure 2 only shows onset points of the heat signals for T_g. Values reported by Fukuoka et al.[53] and Maltini et al.[25] are not considered in this study because they do not specify which isomer of tartaric acid that they used.

We found that pure crystalline levoglucosan undergoes a transition upon heating from a crystal to a plastic crystal at 386 K in both emulsified and bulk samples prior to the final melting at 455 K, in good agreement with values found in the literature.[57−59] The plastic crystal phase forms an orientationally disordered glass upon cooling at 249 K. Similar behavior has previously been observed for caffeine.[60] The transition of the plastic crystal into an orientationally disordered glass is marked by similar relaxation phenomena as the glass transition of the liquid phase.[61−63] For the few materials where both transitions could be observed, the orientionally disordered glass forms either at approximately the same temperature as the glass[64−67] or 6−9 K lower.[66,68] Because a glass transition of the liquid phase was not observed for levoglucosan, we adopt the value of 249 K as T_g.

Single levitated aqueous levoglucosan particles also undergo a transition from liquid to a plastic crystal or a hydrate upon drying, unambiguously marked by the loss of the regular scattering pattern in the EDB experiments or the loss of WGM in optical tweezers experiments. From our experiments, it could not be determined whether a plastic crystal or a hydrate formed. The fact that the particles remained optically trapped for several hours after this transition occurred implies that the shape of the plastic crystal or the hydrate was almost spherical. Using fast drying ramps, some optically tweezed particles could be kept at very dry conditions for several minutes before this phase change occurred. This transition is reversible and has not been observed in EDB experiments at temperatures lower than 243 K, presumably because the liquid forms a glass upon drying at these temperatures rather than a plastic crystal or a hydrate (see Figure 2a), therefore retaining the spherical shape.

The T_g curves in Figure 2 are empirical fits of the Gordon−Taylor equation[69] to the data

$$T_g = \frac{(1 - \mathrm{mfs}) \cdot T_{g1} + \frac{1}{k_{GT}} \cdot \mathrm{mfs} \cdot T_{g2}}{(1 - \mathrm{mfs}) + \frac{1}{k_{GT}} \cdot \mathrm{mfs}} \quad (3)$$

where T_{g1} is the glass transition temperature of pure water, which is taken as 136 K,[70−72] and k_{GT} is a fit parameter that amounts to 3.257 for levoglucosan and to 2.937 for L(+)-tartaric acid. T_{g2} denotes the glass transition temperature of the pure solute and can be obtained from Table 3 for both levoglucosan and L(+)-tartaric acid. The glass transition curve of levoglucosan reported here differs from the one reported by Zobrist et al.[37] because the latter was only based on three data points in a limited concentration range.

Water Activities. Figure 3 shows water activities derived from both bulk measurements at 298 K and EDB measurements at 290.6 K for aqueous levoglucosan solutions and ternary aqueous solutions containing levoglucosan and NH_4HSO_4, $(NH_4)_2SO_4$, and NH_4NO_3 with a 1:1 molar ratio of organic to salt. These results are tabulated in Table 4 in the Appendix.

For all solutes investigated, water activities at lower temperatures were calculated from T_m, T_g', and T_{hom} measurements using the parametrization provided by Murphy and Koop[73] for the water vapor pressure and assuming a temperature-independent water activity difference between T_m and T_{hom} of 0.3125.[74,75] In addition, EDB measurements at 273 and 243 K were carried out for binary aqueous levoglucosan solutions, also shown in Figure 3. These water activity

dx.doi.org/10.1021/jp3055872 | J. Phys. Chem. A 2012, 116, 9954−9968

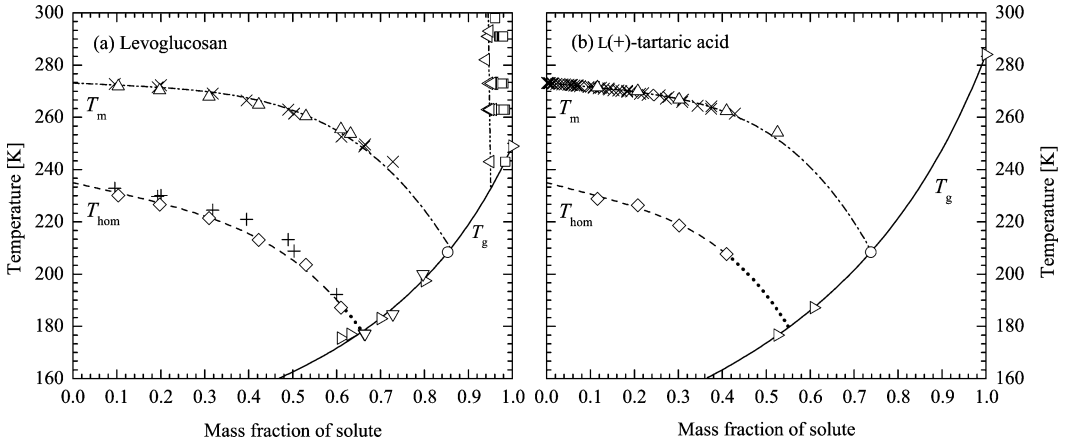

Figure 2. Phase diagrams of (a) levoglucosan and (b) L(+)-tartaric acid. The symbols are (▷) T_g, (△) T_m, (◇) T_{hom}, and (○) T'_g from this study and (▽) T_g, (×) T_m, and (+) T_{hom} from literature data for levoglucosan[37,50] and L(+)-tartaric acid.[54−56] The transition of single levitated particles containing levoglucosan and water into a plastic crystal or a hydrate upon drying is indicated by (□) and the reverse transition by (◁). The solid line represents the T_g curve according to the Gordon−Taylor equation (eq 3), the dashed−dotted line represents the T_m curve (eq 1), the dashed line represents the T_{hom} curve (eq 2), and the dotted line represents the extrapolation of the T_{hom} curve to the intercept with the T_g curve. The experimental uncertainties are within the symbol size.

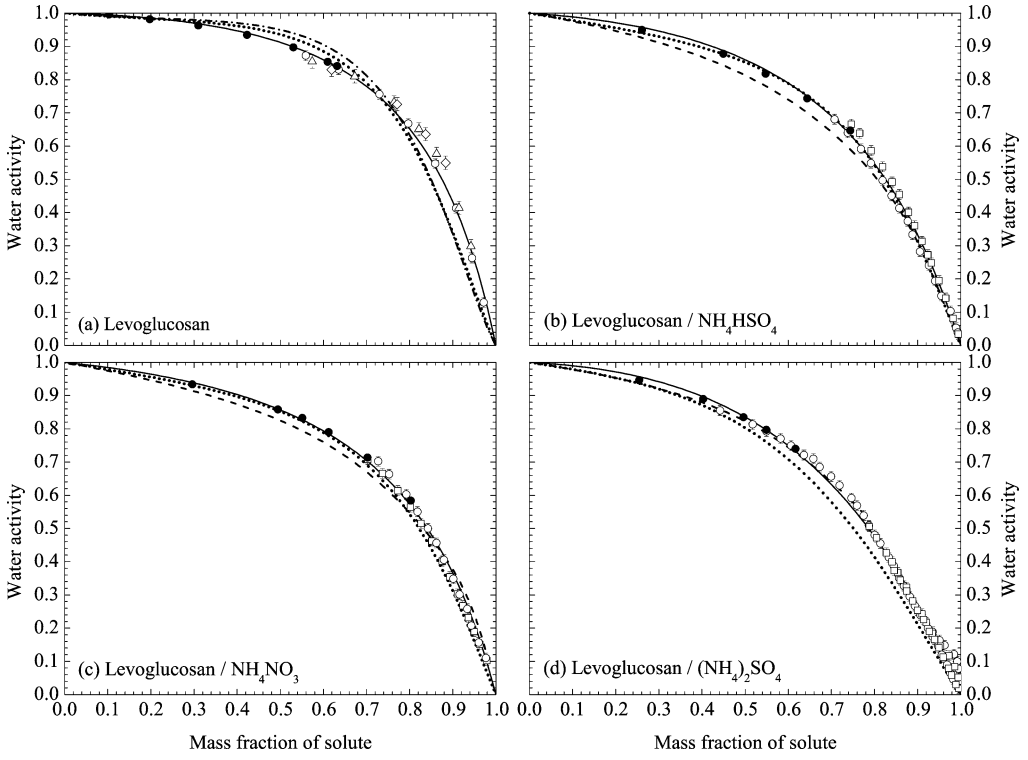

Figure 3. Water activity as a function of mfs of (a) a binary aqueous levoglucosan solution and ternary aqueous solutions containing levoglucosan and one of the inorganic salts, (b) NH_4HSO_4, (c) NH_4NO_3, and (d) $(NH_4)_2SO_4$ with a 1:1 molar ratio of the organic and the salt. The symbols are (●) bulk a_w measurements at 298 K, (○) EDB mass measurements at 290.6 K, (△) EDB mass measurements at 273 K, (◇) EDB mass measurements at 243 K, and (□) EDB radius measurements at 290.6 K from this study. The solid, dotted, dashed, and dashed−dotted lines show the prediction from the fit curve (eq 4), the AIOMFAC model, the ZSR relation, and the UNIFAC model for 298 K, respectively. EDB radius measurements and literature data[6,18] agree with measurements shown in panel (a) and are not shown for reasons of clarity. If not explicitly indicated, the experimental uncertainties are within the symbol size.

measurements at different temperatures from different techniques were fitted to the following empirical expression

$$a_w = \frac{1 - \text{mfs}}{1 + q\cdot\text{mfs} + r\cdot\text{mfs}^2} \quad (4)$$

with

$$q = a_1 + a_2\cdot T + a_3\cdot T^2 \quad (5)$$

and

$$r = a_4 + a_5\cdot T + a_6\cdot T^2 \quad (6)$$

representing the temperature and composition dependence of a_w for each aqueous system. The solid curves in Figure 3 show

dx.doi.org/10.1021/jp3055872 | J. Phys. Chem. A 2012, 116, 9954−9968

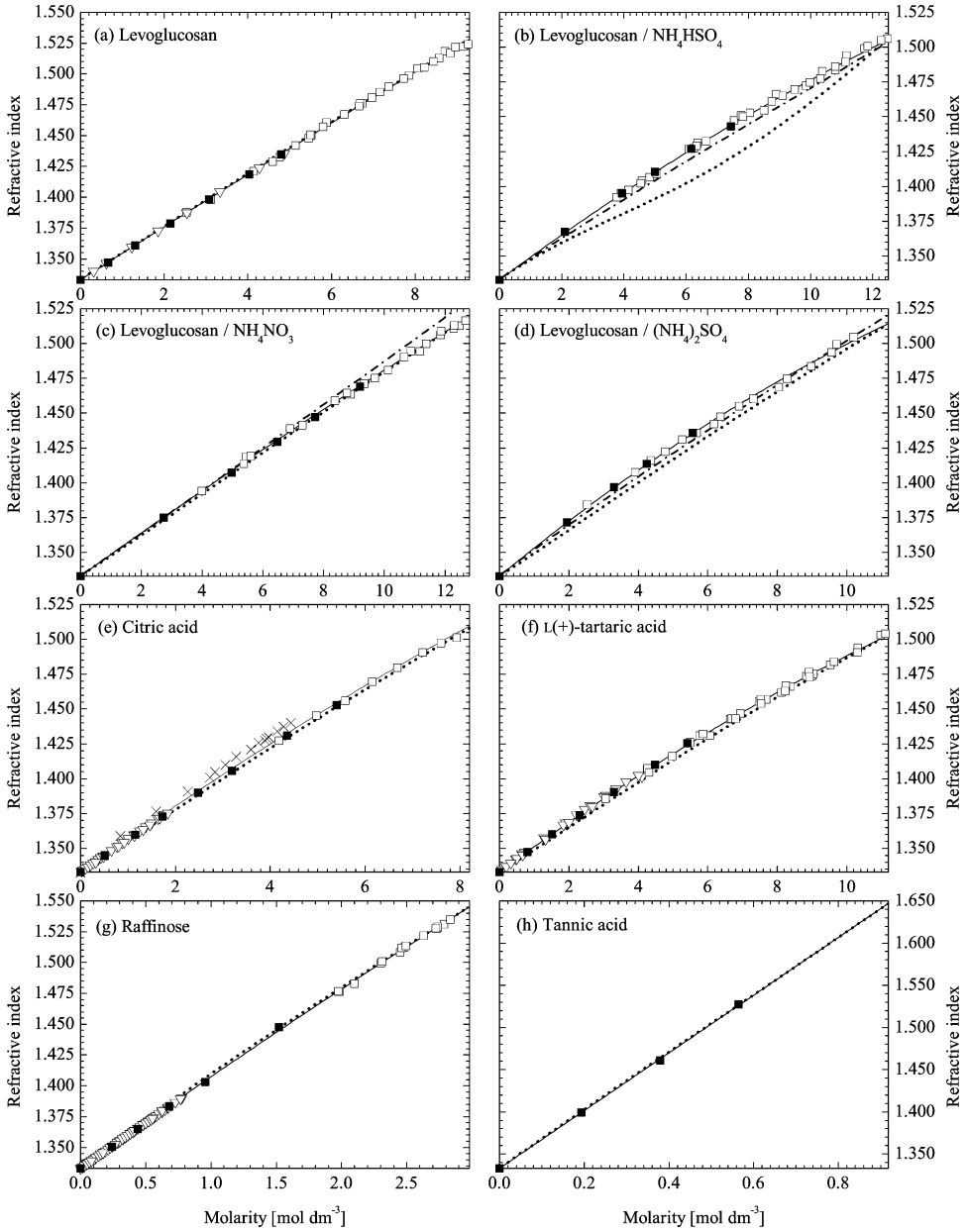

Figure 4. Refractive indices at 589 nm of aqueous mixtures investigated in this study as a function of molarity of the solute at 298 K. The solutes are indicated in each panel. Note that the refractive index scale varies between the solutes and is labeled on the left or right of each panel. The molarity scale for each solute was chosen such that it spans the concentration range from infinite dilution to the pure solute. The symbols are (■) solution refractometry and (□) refractive index measurements from levitated particles from this study and (▽) solution refractometry from the literature for levoglucosan,[17] citric acid,[83,84] L(+)-tartaric acid,[90] and raffinose.[80,91,92] The measurements of Laguerie et al.[82] are indicated by (×) and were not used in the evaluation. The solid, dotted, and dashed−dotted lines represent the parameterzation from eq 8, the predictions according to the additivity rule of the molar refractivities (eq 13), and the prediction according to eq 13, taking the concentration dependence of V^{ϕ} into account. The experimental uncertainties are within the symbol size.

the fit curves for 298 K. Table 2 lists the parameters a_1-a_6 for each solute. The ternary mixtures were only investigated at one temperature (290.6 K) in the EDB. Concentration measurements via radius retrieval from elastic Mie resonance spectroscopy compare well with mass measurements, confirming the parametrizations proposed in Table 1 for the density and refractive index because these are needed to retrieve the radius from Mie resonance spectra measured with the low-resolution LED technique.[38] Because the density and refractive index parametrizations were derived from optical tweezers experiments, this agreement therefore implies that EDB and optical tweezers experiments are consistent.

For the ternary mixtures of NH_4NO_3, the concentration range above mfs > 0.98 could not be investigated because of evaporation of NH_3 and HNO_3 from the solution, as previously observed.[76,77] The mixture containing $(NH_4)_2SO_4$ shows a small but significant hysteresis in the drying and humidifying cycle at a RH lower than 15%. Because neither the WGM nor the two-dimensional angular scattering pattern indicate a solid inclusion that could disturb the spherical symmetry, we conclude that the salt did not effloresce, and levoglucosan did not form a crystal or plastic crystal over the whole humidity range. In addition, this hysteresis cannot be due to kinetic limitations because the particles responded quickly to changes

dx.doi.org/10.1021/jp3055872 | J. Phys. Chem. A 2012, 116, 9954−9968

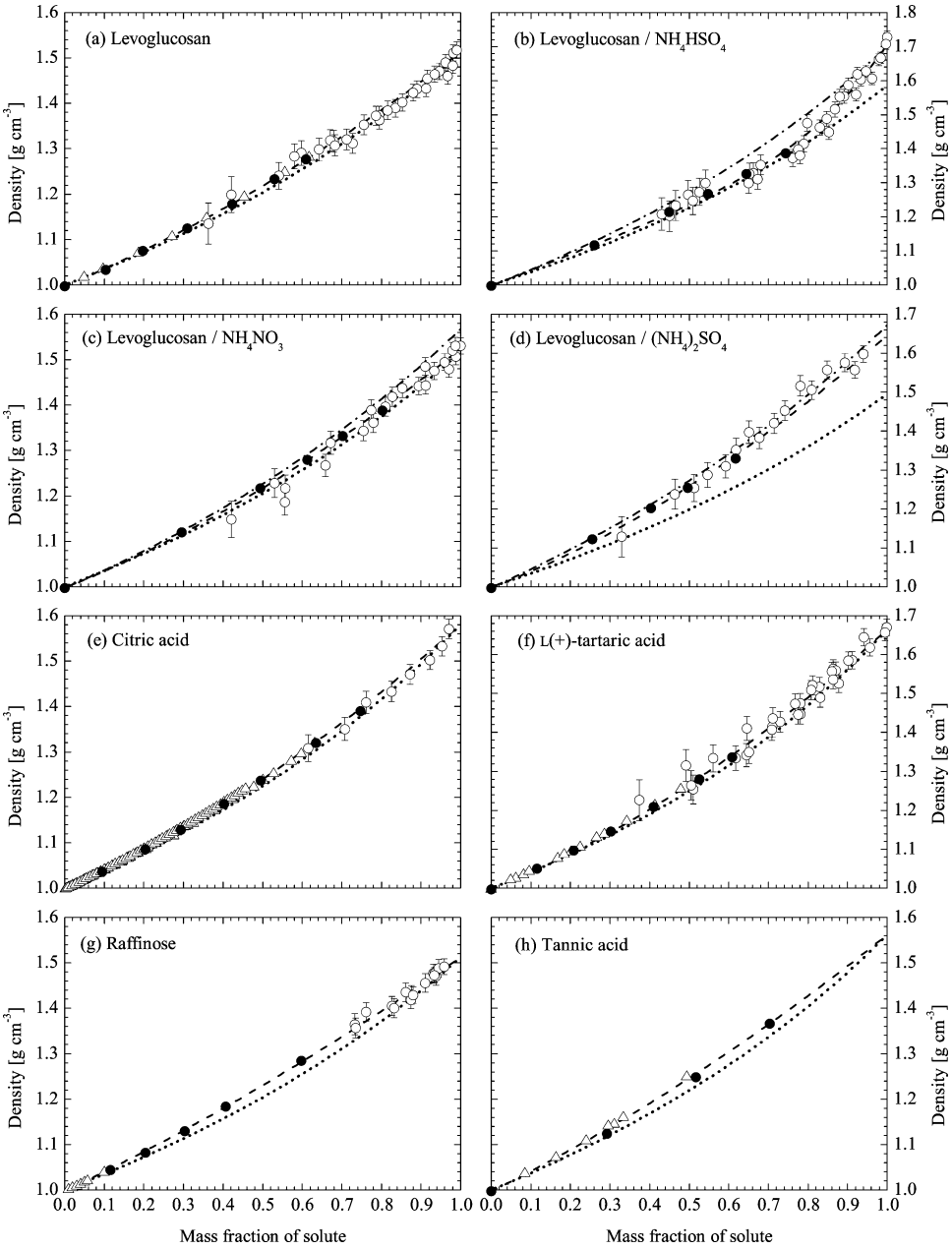

Figure 5. Densities of aqueous mixtures investigated in this study as a function of mass fraction of solute at 298 K. The solutes are indicated in each panel. Note that the density scale varies for different solutes, labeled on the left or the right of each panel. The symbols are (●) solution pycnometry and (○) density measurements from levitated particles from this study and (△) solution refractometry from the literature for levoglucosan,[17] citric acid,[82−84,93−96] L(+)-tartaric acid,[93,97] raffinose,[98−101] and tannic acid.[102] The dashed, dotted, and dashed−dotted lines represent the parametrizations from eq 7, the predictions according to VAR (eq 9), and the prediction according to eq 10. If not explicitly indicated, the experimental uncertainties are within the symbol size.

in RH, even below 15%. At present, we cannot offer an explanation for this behavior. We speculate that this hysteresis could be due to irreversible changes in the water solvation shell of the dissolved substances.

Predictions from the AIOMFAC model[7,30] (Aerosol Inorganic−Organic Mixtures Functional Groups Activity Coefficients; available at http://www.aiomfac.caltech.edu), the UNIFAC model,[31,32] and the ZSR relation[33−35] for the ternary systems are shown in Figure 3 for comparison. The water activities of binary aqueous salt systems for the ZSR relation are taken from Tang and Munkelwitz[27] [$(NH_4)_2SO_4$ and NH_4HSO_4] and from Clegg et al.[78] (NH_4NO_3, available at http://www.aim.env.uea.ac.uk/aim/aim.php), while the water activity of the binary aqueous levoglucosan system is taken from this work.

The thermodynamic model AIOMFAC is a group contribution activity coefficient model combining an ion interaction contribution to the Gibbs excess energy of a system based on a Pitzer-like approach with a short-range contribution from a modified UNIFAC model. This activity coefficient model is designed to enable activity coefficient predictions for liquid organic−inorganic systems from dilute aqueous solutions to mixtures of high ionic strength for temperatures close to 298 K. The AIOMFAC model is described in detail elsewhere.[7,30] We note that the a_w data of the ternary organic−electrolyte systems shown in Figure 3b−d have been used as part of a large

dx.doi.org/10.1021/jp3055872 | J. Phys. Chem. A 2012, 116, 9954−9968

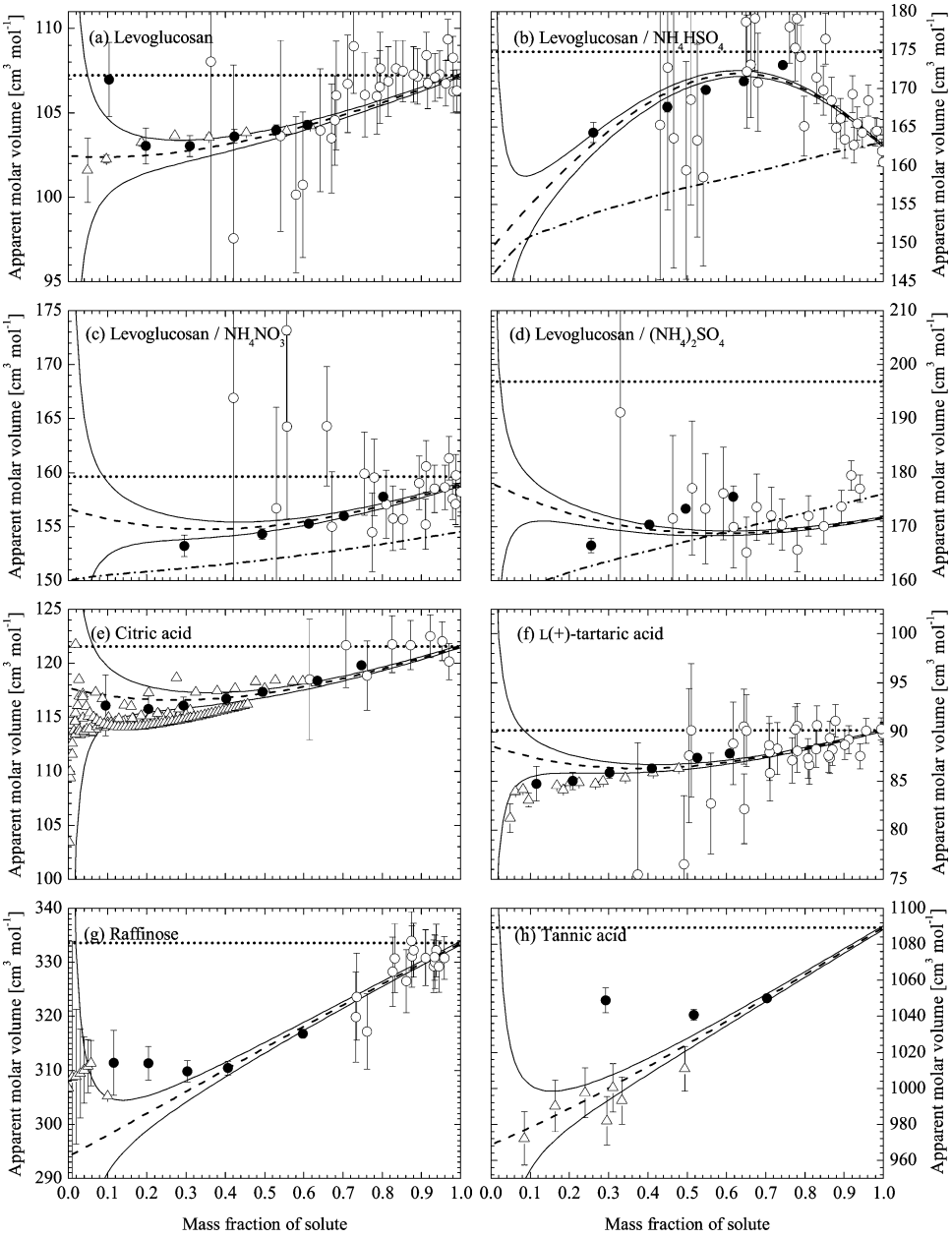

Figure 6. Apparent molar volumes of aqueous mixtures investigated in this study as a function of mass fraction of solute at 298 K. The solutes are indicated in each panel. Note that the apparent molar volume scale varies for different solutes, labeled on the left or the right of each panel. The symbols are (●) solution pycnometry and (○) density measurements from levitated particles from this study and (△) solution refractometry from the literature for levoglucosan,[17] citric acid,[82−84,93−96] L(+)-tartaric acid,[93,97] raffinose,[98−101] and tannic acid.[102] The dashed, dashed−dotted, and dotted lines represent the parametrizations from eqs 7 and 10 and the partial molar volume of the pure liquid solute. The solid lines show the effect of a ±0.0015 g cm^{-3} error in measured density. If not explicitly indicated, the experimental uncertainties are within the symbol size. The uncertainties of literature data of citric acid are not indicated for reasons of clarity.

database to determine organic−ion interation parameters of corresponding functional groups within the AIOMFAC model.[7] The UNIFAC−a_w curve shown in Figure 3a is calculated with the standard UNIFAC model (Fredenslund et al.,[31] based on parameters of Hansen et al.[32]).

Regarding the binary levoglucosan system, the AIOMFAC model predicts higher water activities for mfs below 0.73 and lower water activies for mfs above 0.73, with deviations of up to 0.025 and 0.1, respectively. The UNIFAC model predicts higher water activities in the concentration range between mfs = 0.32 and 0.83 than the AIOMFAC model and therefore shows larger deviations from the measurements than the AIOMFAC model. For the ternary systems, both the AIOMFAC model and the ZSR relation perform reasonably well. The AIOMFAC model underestimates a_w in the systems of $(NH_4)_2SO_4$ and NH_4HSO_4, with deviations of up to 0.08, while the ZSR relation underestimates a_w of the systems of NH_4HSO_4 and NH_4NO_3, with a maximum deviation of 0.05.

In terms of the mass growth factor of an aerosol particle at 90% RH (corresponding to wet particle mass), the percentage difference between the AIOMFAC model and the best fit (eq 4) is 8.7% for the binary levoglucosan systems, and for the ternary systems, the differences are 21.7 (NH_4HSO_4), 4.6 (NH_4NO_3), and 15.9% [$(NH_4)_2SO_4$]. The mass growth factor

dx.doi.org/10.1021/jp3055872 | J. Phys. Chem. A 2012, 116, 9954−9968

Table 3. Measured T_m, T_{hom}, and T_g of Aqueous Organic and Organic–Inorganic Solutions with the Indicated mfs[a]

levoglucosan				L(+)-tartaric acid				levoglucosan/NH_4HSO_4		
mfs	T_m [K]	T_{hom} [K]	T_g [K]	mfs	T_m [K]	T_{hom} [K]	T_g [K]	mfs	T_m [K]	T_{hom} [K]
0.103	271.9	230.1		0.116	271.5	228.8		0.261	266.3	219.8
0.197	270.3	226.6		0.208	270.1	226.4		0.450	258.0	200.2
0.310	267.9	221.4		0.302	266.9	218.6		0.548	250.9	175.5
0.423	264.9	213.1		0.410	262.5	207.6				
0.530	260.4	203.5		0.526	254.2		176.7			
0.610	255.5	187.2	175.5	0.608			187.5			
0.632	253.7		176.9	1.000			284.1			
0.701			182.9							
0.801			197.5							
1.000			249.0[b]							

levoglucosan/$(NH_4)_2SO_4$			levoglucosan/NH_4NO_3			tannic acid	
mfs	T_m [K]	T_{hom} [K]	mfs	T_m [K]	T_{hom} [K]	mfs	T_m [K]
0.255	266.5	221.4	0.296	265.9	220.8	0.065	273.11[c]
0.403	260.3	209.2	0.494	259.0	210.2	0.117	273.11[c]
0.497	245.7	198.0	0.612	252.7	199.0	0.259	273.09[c]
			0.803	237.2		0.703	270.8

[a]Raffinose and citric acid are not listed here because their phase transitions have been investigated in previous studies.[37,103−105] [b]Glass transition temperature of the plastic crystal. [c]From ref 112.

derived from the ZSR relation deviates from the best fit by 29.7 (NH_4HSO_4), 21.5 (NH_4NO_3), and 11.3% [$(NH_4)_2SO_4$]. We note that the best fit curve shows slight deviations from the measured data points in the corresponding concentration range, explaining a part of the percentage difference stated above.

Reasons for the deviation of the AIOMFAC model predictions for mixtures containing levoglucosan are discussed in Zuend et al.[7] The strength of the AIOMFAC model compared to the ZSR relation is that it consistently predicts the activity coefficients of water and all other components present in the solution. Note that in contrast to the ZSR approach, the AIOMFAC model was not specifically fitted to the present data; rather, its predictions are based on a group contribution concept and model parametrization using a large database of organic–inorganic systems, making it more versatile than the ZSR approach. Moreover, ZSR a_w calculations become ambiguous for mixtures containing more than one salt, as shown in Zuend et al.[30] Nevertheless, the comparison shows that the simple ZSR relation can yield comparable accuracy for predictions of water activities in specific systems, given that necessary binary water activity parametrizations of the subsystems are available.

The a_w parametrizations of citric acid and L(+)-tartaric acid are based on bulk a_w measurements from the literature and T_m, T_g', and T_{hom} measurements from this study and from the literature (see Table 2). Low RH data measured in EDB experiments from Peng et al.[4,5] were not considered because it is not clear whether these particles were fully equilibrated with respect to the RH. Recent studies highlight the kinetic limitations that some systems exhibit at low RH, which could be an explanation of the residual water content.[38,79−81]

Densities and Refractive Indices. The radii and refractive indices of optically tweezed particles equilibrated at different RHs at 298 K were calculated from the stimulated Raman fingerprint, as described in the method section. The refractive indices were then related to the molarity of the solute in the liquid particle by comparing the refractive index of the optically tweezed particle to bulk refractive index measurements with known molarity in the corresponding concentration range. The molarities of optically tweezed particles in the concentration range where no bulk refractive index measurements are available were calculated using the radius of the particles (molarity scales with the third power of the radius). Figure 4 shows the refractive indices of all investigated aqueous solutions as a function of molarity of the solute. The uncertainties in the refractive index retrieval from single levitated microdroplets are within the symbol size in Figure 4. For raffinose, no refractive indices measurements from optically tweezed particles were available in the concentration range of the bulk refractive index measurements. Thus, the concentration dependence of the bulk refractive index measurements was extrapolated over the molarity range between 1.521 and 1.981 mol dm^{-3} or, in terms of mfs, between 0.598 and 0.732.

The relationship between the refractive index and mfs was obtained from the bulk refractive index measurements, where mfs is known, and the highest refractive index measurement from optically tweezed particles, that is, at 0% RH, where mfs = 1. For citric acid and raffinose, a measurement with mfs = 1 could not be obtained because of kinetic limitations at low RH. For the ternary system of $(NH_4)_2SO_4$, a measurement with mfs = 1 was not possible because of the hysteresis effect at low RH described above. Therefore, the refractive index and mfs of the particle fully equilibrated at the lowest RH possible were used in these three systems instead.

When the dependence of the refractive index on mfs is known, it can be applied to find the mfs of the optically tweezed particles according to their index of refraction. Combined with the known molarity of these particles, one obtains the density of the aqueous solution of the particle. This procedure results in smaller errors than when using the relationship between a_w and mfs.

Figure 5 shows the densities of all investigated aqueous solutions as a function of mfs. The error bars of the densities derived from optical tweezers experiments are calculated from the uncertainties in the refractive index determination, which specifies the error in mfs used to calculate ρ. In addition, the error in the simultaneous radius determination has been taken

Table 4. a_w Measurements at Different Temperatures[a]

levoglucosan									
298 K (bulk)		290.6 K (mass)		290.6 K (LED)		273 K (mass)		243 K (mass)	
mfs	a_w	mfs	a_w	mfs	a_w	mfs	a_w	mfs	a_w
0.610	0.854	0.972	0.130	0.976	0.146	0.943	0.299	0.883	0.550
0.531	0.897	0.945	0.263	0.950	0.247	0.915	0.414	0.837	0.636
0.423	0.935	0.907	0.413	0.921	0.348	0.863	0.577	0.771	0.726
0.310	0.963	0.859	0.547	0.890	0.447	0.822	0.651	0.619	0.830
0.197	0.982	0.797	0.668	0.855	0.539	0.764	0.731		
0.103	0.996	0.730	0.757	0.810	0.631	0.673	0.810		
0.632	0.841	0.635	0.831	0.750	0.733	0.574	0.855		
		0.559	0.872	0.657	0.821				
				0.514	0.894				

levoglucosan/$(NH_4)_2SO_4$											
298 K (bulk)		290.6 K (mass)[b]		290.6 K (mass)[c]		290.6 K (mass)[c]		290.6 K (LED)[b]		290.6 K (LED)[c]	
mfs	a_w	mfs	a_w	mfs	a_w	mfs	a_w	mfs	a_w	mfs	a_w
0.617	0.740	0.998	0.031	0.442	0.855	0.814	0.455	0.999	0.021	0.996	0.019
0.497	0.835	0.998	0.053	0.518	0.813	0.833	0.413	0.995	0.051	0.989	0.030
0.403	0.890	0.995	0.078	0.549	0.792	0.845	0.388	0.986	0.084	0.979	0.057
0.255	0.947	0.992	0.010	0.582	0.771	0.857	0.351	0.973	0.117	0.972	0.079
0.550	0.797	0.984	0.121	0.607	0.750	0.869	0.327	0.953	0.145	0.959	0.113
		0.962	0.149	0.636	0.721	0.882	0.296	0.933	0.184	0.950	0.141
		0.951	0.164	0.658	0.710	0.894	0.267	0.920	0.217	0.939	0.165
		0.935	0.189	0.673	0.685	0.907	0.239	0.910	0.243	0.927	0.191
				0.700	0.656	0.924	0.200	0.874	0.323	0.914	0.225
				0.719	0.630	0.935	0.174	0.854	0.367	0.900	0.253
				0.747	0.591	0.947	0.146	0.841	0.400	0.888	0.282
				0.759	0.569	0.956	0.120	0.827	0.427	0.875	0.312
				0.775	0.539	0.968	0.090	0.805	0.472	0.860	0.345
				0.787	0.509	0.976	0.065	0.788	0.506	0.846	0.373
				0.801	0.481	0.983	0.046				
						0.993	0.023				

levoglucosan/NH_4NO_3						levoglucosan/NH_4HSO_4					
298 K (bulk)		290.6 K (mass)		290.6 K (LED)		298 K (bulk)		290.6 K (mass)		290.6 K (LED)	
mfs	a_w	mfs	a_w	mfs	a_w	mfs	a_w	mfs	a_w	mfs	a_w
0.803	0.584	0.727	0.702	0.703	0.707	0.644	0.744	0.708	0.681	0.994	0.034
0.702	0.714	0.753	0.664	0.737	0.666	0.548	0.818	0.738	0.641	0.982	0.082
0.612	0.790	0.792	0.603	0.773	0.614	0.450	0.878	0.769	0.592	0.966	0.143
0.494	0.858	0.819	0.550	0.801	0.565	0.261	0.950	0.792	0.549	0.950	0.195
0.296	0.934	0.842	0.500	0.827	0.515	0.744	0.647	0.819	0.497	0.932	0.248
		0.862	0.457	0.851	0.463			0.839	0.450	0.924	0.273
		0.880	0.406	0.876	0.402			0.857	0.413	0.910	0.313
		0.901	0.348	0.893	0.354			0.877	0.374	0.893	0.360
		0.916	0.302	0.911	0.303			0.888	0.333	0.879	0.401
		0.934	0.258	0.923	0.268			0.905	0.283	0.858	0.454
		0.943	0.207	0.936	0.231			0.926	0.240	0.841	0.492
		0.960	0.157	0.949	0.190			0.941	0.194	0.819	0.537
		0.977	0.110	0.963	0.151			0.955	0.149	0.792	0.586
				0.980	0.103			0.976	0.104	0.766	0.638
								0.989	0.054	0.746	0.666
								0.993	0.039		

[a]The values for a_w depending on mfs were obtained from different techniques that are indicated: (bulk) bulk a_w measurements; (mass) EDB mass measurements; (LED) EDB radius measurements using the LED. The uncertainties are ±0.003 for bulk a_w measurements and ±0.02 for EDB mass and radius measurements. Note that more data on water activities are available from T_m and T_{hom} measurements, as described in the text. [b]Water adsorption. [c]Water desorption.

dx.doi.org/10.1021/jp3055872 | J. Phys. Chem. A 2012, 116, 9954−9968

Table 5. ρ and n of the Solutes Investigated in This Study Depending on mfs and M[a]

citric acid				raffinose				levoglucosan/NH_4NO_3			
	ρ	M			ρ	M			ρ	M	
mfs	g cm^{-3}	mol dm^{-3}	n	mfs	g cm^{-3}	mol dm^{-3}	n	mfs	g cm^{-3}	mol dm^{-3}	n
0.095	1.0362	0.511	1.3446	0.116	1.0436	0.240	1.3504	0.296	1.1194	2.735	1.3749
0.203	1.0852	1.149	1.3597	0.204	1.0820	0.437	1.3650	0.494	1.2165	4.967	1.4072
0.293	1.1287	1.723	1.3729	0.303	1.1296	0.678	1.3831	0.612	1.2800	6.474	1.4295
0.402	1.1850	2.481	1.3899	0.407	1.1831	0.954	1.4031	0.702	1.3317	7.720	1.4472
0.496	1.2367	3.190	1.4056	0.598	1.2840	1.521	1.4474	0.803	1.3876	9.200	1.4690
0.634	1.3200	4.357	1.4311	0.732	1.365 ± 0.023	1.981	1.4762	0.421	1.148 ± 0.040	3.991	1.3942
0.747	1.3894	5.399	1.4530	0.735	1.356 ± 0.022	1.976	1.4769	0.530	1.228 ± 0.032	5.375	1.4138
0.615	1.308 ± 0.029	4.187	1.4273	0.761	1.392 ± 0.021	2.099	1.4831	0.557	1.187 ± 0.029	5.454	1.4188
0.707	1.350 ± 0.025	4.970	1.4452	0.827	1.405 ± 0.021	2.302	1.4995	0.558	1.217 ± 0.030	5.603	1.4190
0.761	1.409 ± 0.024	5.581	1.4561	0.832	1.401 ± 0.021	2.310	1.5010	0.659	1.267 ± 0.025	6.897	1.4390
0.825	1.433 ± 0.023	6.155	1.4695	0.861	1.435 ± 0.021	2.450	1.5085	0.671	1.317 ± 0.025	7.301	1.4415
0.873	1.471 ± 0.022	6.682	1.4798	0.874	1.419 ± 0.019	2.459	1.5119	0.755	1.344 ± 0.022	8.377	1.4591
0.922	1.502 ± 0.021	7.212	1.4907	0.875	1.429 ± 0.020	2.480	1.5122	0.775	1.389 ± 0.023	8.885	1.4634
0.953	1.533 ± 0.021	7.600	1.4975	0.880	1.429 ± 0.018	2.493	1.5135	0.779	1.361 ± 0.021	8.760	1.4644
0.970	1.571 ± 0.021	7.931	1.5014	0.911	1.456 ± 0.020	2.628	1.5217	0.810	1.397 ± 0.021	9.343	1.4712
				0.931	1.477 ± 0.020	2.727	1.5273	0.828	1.418 ± 0.021	9.692	1.4751
				0.933	1.473 ± 0.017	2.725	1.5280	0.853	1.437 ± 0.020	10.117	1.4808
				0.935	1.477 ± 0.020	2.736	1.5283	0.894	1.442 ± 0.019	10.645	1.4904
				0.938	1.471 ± 0.020	2.735	1.5292	0.911	1.485 ± 0.019	11.170	1.4943
				0.944	1.488 ± 0.020	2.785	1.5310	0.912	1.443 ± 0.019	10.871	1.4947
				0.958	1.492 ± 0.017	2.833	1.5348	0.933	1.476 ± 0.019	11.374	1.4997
								0.960	1.495 ± 0.019	11.852	1.5062
								0.971	1.479 ± 0.018	11.862	1.5088
								0.979	1.520 ± 0.018	12.290	1.5108
								0.987	1.531 ± 0.018	12.483	1.5128
								0.988	1.507 ± 0.018	12.298	1.5131
								1.000	1.531 ± 0.018	12.676	1.5166
L(+)-tartaric acid				Levoglucosan				Levoglucosan/NH_4HSO_4			
	ρ	M			ρ	M			ρ	M	
mfs	g cm^{-3}	mol dm^{-3}	n	mfs	g cm^{-3}	mol dm^{-3}	n	mfs	g cm^{-3}	mol dm^{-3}	n
0.116	1.0503	0.812	1.3474	0.103	1.0336	0.657	1.3471	0.261	1.1161	2.098	1.3674
0.208	1.0963	1.518	1.3602	0.197	1.0748	1.308	1.3607	0.450	1.2139	3.937	1.3952
0.302	1.1458	2.305	1.3739	0.310	1.1247	2.148	1.3787	0.548	1.2671	5.005	1.4106
0.410	1.2085	3.300	1.3906	0.423	1.1780	3.074	1.3985	0.644	1.3262	6.163	1.4269
0.526	1.2794	4.483	1.4099	0.530	1.2329	4.034	1.4185	0.744	1.3863	7.438	1.4430
0.608	1.3356	5.414	1.4256	0.610	1.2763	4.802	1.4349	0.431	1.208 ± 0.047	3.760	1.3924
0.375	1.226 ± 0.052	3.060	1.3855	0.363	1.135 ± 0.045	2.541	1.3876	0.450	1.202 ± 0.045	3.906	1.3952
0.492	1.315 ± 0.041	4.311	1.4045	0.421	1.199 ± 0.040	3.112	1.3980	0.465	1.233 ± 0.044	4.141	1.3975
0.505	1.264 ± 0.038	4.255	1.4068	0.541	1.241 ± 0.030	4.140	1.4210	0.497	1.265 ± 0.042	4.535	1.4023
0.510	1.254 ± 0.037	4.262	1.4076	0.581	1.283 ± 0.028	4.596	1.4290	0.509	1.247 ± 0.040	4.578	1.4042
0.560	1.334 ± 0.035	4.976	1.4161	0.598	1.291 ± 0.027	4.757	1.4325	0.525	1.273 ± 0.040	4.825	1.4067
0.617	1.334 ± 0.031	5.483	1.4260	0.643	1.298 ± 0.025	5.147	1.4420	0.540	1.299 ± 0.039	5.064	1.4091
0.644	1.342 ± 0.030	5.760	1.4310	0.671	1.319 ± 0.024	5.455	1.4480	0.650	1.299 ± 0.030	6.090	1.4271
0.645	1.410 ± 0.031	6.062	1.4311	0.680	1.317 ± 0.024	5.522	1.4500	0.652	1.326 ± 0.031	6.236	1.4275
0.651	1.350 ± 0.030	5.857	1.4322	0.682	1.307 ± 0.024	5.501	1.4505	0.662	1.329 ± 0.030	6.342	1.4291
0.708	1.407 ± 0.028	6.640	1.4428	0.712	1.320 ± 0.023	5.799	1.4571	0.673	1.311 ± 0.029	6.366	1.4312
0.710	1.415 ± 0.028	6.697	1.4432	0.727	1.312 ± 0.022	5.886	1.4605	0.681	1.352 ± 0.029	6.643	1.4325
0.711	1.436 ± 0.028	6.798	1.4432	0.756	1.353 ± 0.022	6.307	1.4670	0.761	1.373 ± 0.025	7.538	1.4473
0.729	1.427 ± 0.027	6.936	1.4467	0.786	1.373 ± 0.021	6.658	1.4740	0.776	1.398 ± 0.024	7.824	1.4502
0.767	1.473 ± 0.026	7.533	1.4541	0.794	1.373 ± 0.020	6.729	1.4759	0.780	1.380 ± 0.024	7.764	1.4510
0.776	1.446 ± 0.025	7.477	1.4558	0.795	1.363 ± 0.020	6.684	1.4760	0.789	1.414 ± 0.024	8.055	1.4529
0.781	1.447 ± 0.025	7.526	1.4567	0.816	1.384 ± 0.020	6.969	1.4810	0.799	1.476 ± 0.025	8.503	1.4548
0.781	1.475 ± 0.025	7.677	1.4568	0.835	1.389 ± 0.020	7.156	1.4855	0.830	1.462 ± 0.022	8.752	1.4612
0.808	1.509 ± 0.025	8.118	1.4621	0.852	1.403 ± 0.019	7.374	1.4897	0.848	1.488 ± 0.022	9.100	1.4651
0.812	1.521 ± 0.025	8.228	1.4630	0.880	1.424 ± 0.018	7.729	1.4965	0.853	1.448 ± 0.022	8.908	1.4662
0.829	1.517 ± 0.024	8.376	1.4664	0.890	1.432 ± 0.019	7.859	1.4989	0.868	1.516 ± 0.022	9.488	1.4696
0.831	1.489 ± 0.024	8.246	1.4669	0.913	1.433 ± 0.018	8.066	1.5045	0.880	1.553 ± 0.022	9.856	1.4724
0.860	1.557 ± 0.024	8.923	1.4729	0.916	1.455 ± 0.018	8.222	1.5054	0.891	1.554 ± 0.021	9.984	1.4749

dx.doi.org/10.1021/jp3055872 | J. Phys. Chem. A 2012, 116, 9954−9968

Table 5. continued

L(+)-tartaric acid				Levoglucosan				Levoglucosan/NH_4HSO_4			
	ρ	M			ρ	M			ρ	M	
mfs	g cm^{-3}	mol dm^{-3}	n	mfs	g cm^{-3}	mol dm^{-3}	n	mfs	g cm^{-3}	mol dm^{-3}	n
0.864	1.536 ± 0.023	8.837	1.4737	0.934	1.464 ± 0.018	8.439	1.5100	0.901	1.587 ± 0.020	10.320	1.4776
0.864	1.564 ± 0.023	9.002	1.4737	0.946	1.471 ± 0.018	8.583	1.5130	0.922	1.559 ± 0.020	10.371	1.4828
0.870	1.559 ± 0.023	9.036	1.4750	0.962	1.490 ± 0.018	8.841	1.5171	0.925	1.618 ± 0.020	10.797	1.4835
0.878	1.525 ± 0.023	8.918	1.4766	0.968	1.460 ± 0.018	8.714	1.5185	0.934	1.603 ± 0.019	10.801	1.4859
0.902	1.584 ± 0.023	9.523	1.4819	0.981	1.483 ± 0.017	8.970	1.5218	0.947	1.628 ± 0.018	11.118	1.4895
0.912	1.586 ± 0.022	9.638	1.4840	0.981	1.511 ± 0.018	9.144	1.5220	0.962	1.606 ± 0.018	11.150	1.4939
0.941	1.645 ± 0.022	10.310	1.4905	0.990	1.517 ± 0.018	9.266	1.5243	0.979	1.662 ± 0.018	11.736	1.4990
0.957	1.618 ± 0.022	10.316	1.4941					0.984	1.667 ± 0.016	11.828	1.5006
0.995	1.657 ± 0.021	10.981	1.5029					0.996	1.708 ± 0.016	12.272	1.5048
0.999	1.670 ± 0.021	11.118	1.5040					1.000	1.728 ± 0.018	12.471	1.5063

Levoglucosan/$(NH_4)_2SO_4$				Tannic Acid			
	ρ	M			ρ	M	
mfs	g cm^{-3}	mol dm^{-3}	n	mfs	g cm^{-3}	mol dm^{-3}	n
0.255	1.1216	1.941	1.3716	0.292	1.1234	0.193	1.3991
0.403	1.2019	3.292	1.3969	0.516	1.2485	0.379	1.4609
0.497	1.2542	4.232	1.4136	0.703	1.3665	0.565	1.5273
0.617	1.3295	5.574	1.4359				
0.330	1.128 ± 0.051	2.529	1.3843				
0.512	1.254 ± 0.035	4.363	1.4162				
0.546	1.288 ± 0.032	4.782	1.4226				
0.618	1.351 ± 0.030	5.676	1.4360				
0.651	1.397 ± 0.029	6.182	1.4423				
0.677	1.383 ± 0.028	6.363	1.4475				
0.715	1.420 ± 0.026	6.897	1.4551				
0.741	1.453 ± 0.025	7.320	1.4606				
0.781	1.516 ± 0.026	8.047	1.4688				
0.809	1.506 ± 0.024	8.279	1.4749				
0.849	1.557 ± 0.023	8.977	1.4836				
0.893	1.576 ± 0.023	9.561	1.4937				
0.918	1.557 ± 0.021	9.716	1.4996				
0.940	1.598 ± 0.021	10.202	1.5047				

[a]Measurements where the error of the density is indicated are derived from optical tweezers measurements by simultaneous determination of the radius and the refractive index. While the error in the refractive index in these experiments is 0.0025, the error in the density was calculated as described in the text. The uncertainties in bulk experiments are 0.0002 for the refractive index and 0.0015 g cm^{-3} for the density.

into account, which provides the error with respect to the molarity. The uncertainties in the solution pycnometry are within the symbol size. All density and refractive index measurements carried out in this work are tabulated in Table 5 in the Appendix.

Our measurements generally agree with values reported in the literature for both densities and refractive indices but cover a wider range of concentrations. All solutes mentioned above except tannic acid were investigated in optical tweezers. Tannic acid absorbs at the wavelength of illumination and thus could not be trapped in the focus of the laser. Note that refractive index measurements on aqueous citric acid solutions by Laguerie et al.[82] were not used for the parametrization because their values deviate significantly from our measurements and other measurements reported in the literature.[83,84]

The following equations were used to fit our density and refractive index data to the measured points shown in Figures 4 and 5 at 298 K and are represented by the solid and dashed lines, respectively:

$$\rho = 0.9971 + d_1 \cdot \mathrm{mfs} + d_2 \cdot \mathrm{mfs}^2 \quad (7)$$

$$n = 1.333 + n_1 \cdot M + n_2 \cdot M^2 \quad (8)$$

The parameters d_1, d_2, n_1, and n_2 are listed in Table 1 for all investigated solutes. The relationship between mfs and n is not listed in Table 1 because it can directly be deduced from the parametrizations given for n and ρ.

Also shown in Figure 5 are predictions from the volume additivity rule (VAR) of the molar volumes of the pure solutes (V) for comparison.

$$\rho = \frac{\sum_i x_i \cdot M_w^i}{\sum_i x_i \cdot V_i} \quad (9)$$

where x_i and M_w^i denote the mole fraction and molar mass of component i, respectively. The molar volumes of the organics derived from our measurements are listed in Table 1. For the ternary systems, the predictions from the additivity rule of the apparent molar volumes[85] (V^ϕ) are also shown.

$$\rho = \frac{\sum_i x_i \cdot M_w^i}{\sum_i x_i \cdot V_i^\phi(\mathrm{mfs}_i)} \quad (10)$$

dx.doi.org/10.1021/jp3055872 | J. Phys. Chem. A 2012, 116, 9954−9968

where $V_i^{\phi}(\mathrm{mfs}_i)$ denotes the apparent molar volume of component i in the binary aqueous solutions according to its mass fraction in the ternary solution. The apparent molar volumes calculated from our density measurements and literature data are shown in Figure 6 in the Appendix. Equation 10 takes interactions between water and the two solute molecules into account. The apparent molar volumes of the salts were taken from Clegg and Wexler,[86,87] the one of levoglucosan from this study (the apparent molar volume of water is, per definition, invariant with concentration).

The VAR only slightly underestimates the densities of aqueous solutions of all binary solutions investigated and at intermediate concentrations of the ternary mixture of levoglucosan and NH_4NO_3. Thus, the apparent molar volume is slightly higher than the molar volume due to molecular interactions in these cases. The prediction of the density from the VAR is significantly lower than bulk and microdroplet measurements for highly concentrated ternary mixtures of NH_4HSO_4 and over all concentrations of the ternary mixtures of $(NH_4)_2SO_4$, while the prediction from eq 10 shows better agreement with the measurements in this concentration range. This agreement suggests that the concentration dependence of V^{ϕ} in the ternary systems is similar to the one in the binary aqueous solutions.

For lower temperatures, we assume that at 0 K, the density of the supercooled melt is equal to the density of the crystal at 298 K.[86,87] The density of the aqueous solution as a function of composition and temperature can then be calculated as

$$\rho(T, \mathrm{mfs}) = \rho_r(\mathrm{mfs}) + \frac{T_r - T}{T_r}\cdot(\rho_c - \rho_m)\cdot\mathrm{mfs} \tag{11}$$

where $\rho_r(\mathrm{mfs})$ denotes the density of the aqueous solution according to its concentration at the reference temperature T_r of 298 K, and ρ_c and ρ_m represent the densities of the crystal and the melt of the pure solute at 298 K, respectively. Table 1 lists ρ_c and provides the parametrizations to calculate ρ_m (i.e., eq 7 with mfs = 1).

From the densities and refractive indicies, the molar refractivity, R, can be obtained according to the following equation and is also listed in Table 1 for each solute:[88,89]

$$R = \frac{V(n^2 - 1)}{n^2 + 2} \tag{12}$$

For the ternary mixtures, V and R are derived by treating the two different solute molecules as one molecule with the combined molar weight. These experimentally observed V and R are compared to the theoretical V and R derived from the sum of V and R of the individual solutes, respectively, indicated in parentheses in Table 1. While the deviations in the molar refractivity between the experimental and the theoretical value are small, the deviations in the molar volumes are large for the ternary solutions containing NH_4HSO_4 and $(NH_4)_2SO_4$. If one assumes that the apparent molar volume of levoglucosan is independent of concentration, the variation in the apparent molar volume of the two salts in the ternary mixtures roughly corresponds to the variation also observed in binary aqueous solutions of NH_4HSO_4 and $(NH_4)_2SO_4$.[86,87]

When the molar refractivities of all substances present in a solution and their mole fractions are known, the molar refractivity of the solution can be calculated according to the additivity rule of the molar refractivities.

$$R = \sum_i R_i x_i \tag{13}$$

Then, the refractive index of the solution can be calculated according to eq 12. These predictions are represented by the dotted lines in Figure 4. Apart from the ternary mixtures of NH_4HSO_4 and $(NH_4)_2SO_4$, the additivity rule of the molar refractivities predicts the refractive indices as a function of the molarity of the solute accurately. When the variations of V^{ϕ} with concentration are taken into account in the three ternary systems, one finds better agreement for the mixtures containing NH_4HSO_4 and $(NH_4)_2SO_4$ (shown by the dashed−dotted lines in Figure 4b−d).

CONCLUSIONS

Single levitated microdroplets of atmospherically relevant composition have been investigated in bulk measurements as well as in optical tweezers and in an electrodynamic balance at various RHs and temperatures. These experiments cover new mixtures and a larger concentration range than those reported previously in the literature. The resonant wavelengths in the light scattered by these particles allows the size and refractive index to be determined simultaneously with considerable accuracy. Combined with bulk solution pycnometry, the density of the supersaturated aqueous solutions could be calculated via simultaneous refractive index and radius determination of optically tweezed particles. Differential scanning calorimetry was used to detect phase transitions of the investigated solutions, from which the temperature dependence of the water activity at known compositions could be inferred. Parameterizations of the measured and derived thermodynamic and optical properties provided in this work should find application in thermodynamic and atmospheric aerosol models as well as in food science.

The measurements carried out in the electrodynamic balance and in optical tweezers showed consistent results for the aqueous droplets investigated in this study. This consistency implies that these two different techniques do not influence the thermodynamic and optical properties of the levitated aqueous droplets, with one requiring levitation of charged droplets and the other trapping with light.

Our water activity measurements show that the AIOMFAC model performs slightly better than the UNIFAC model for binary aqueous levoglucosan solutions. We found that both the Zdanovskii−Stokes−Robinson relation and the AIOMFAC model predict the water activities of the aqueous droplets reasonably well, with associated errors in terms of water activities of less than 0.05 in most cases. The mass growth factor at 90% RH predicted by these two approaches deviates from the best fit by up to 22% for the AIOMFAC model and up to 30% for the ZSR relation. Although a part of these deviations can be explained by uncertainties of the best fit, this indicates room for improvement. The measured data and parametrizations of this study allow application of a specific ZSR relation to systems like the ternary levoglucosan and salt mixtures. In addition, our measurements aid in the further development and evaluation of more general thermodynamic models like the AIOMFAC model.

The additivity rules of the molar volumes and the molar refractivities produce satisfying predictions for the solution density and refractive index for all investigated systems except the two ternary mixtures of the salts NH_4HSO_4 and

dx.doi.org/10.1021/jp3055872 | J. Phys. Chem. A 2012, 116, 9954−9968

$(NH_4)_2SO_4$, where the concentration dependence of the apparent molar volume explains the observed deviation.

APPENDIX

Figure 6 displays the apparent molar volumes calculated from our measurements and from literature data and compares these values to the fit curves from eq 7. Our bulk measurements compare well with literature data except for the tannic acid, for which the preparation reported in the literature was different from ours.[102] The scatter in the reported apparent molar volumes is larger for our investigated systems than that, for example, for some aqueous salt solutions, for which more accurate measurements are often available.[86,87] The fit curves from eq 7 show deviations from the measurements over some concentration ranges where the simple second-order polynomial form of this equation cannot represent the measurements. However, a more precise density parametrization is beyond the scope of this paper.

Density measurements from levitated particles have a large error in the apparent molar volume scale, which is not surprising. The bulk density measurement of the aqueous levoglucosan solution with mfs = 0.103 seems to be erroneous. However, this single measurement only marginally affects the parametrization.

All values experimentally determined are tabulated in Tables 3−5.

AUTHOR INFORMATION

Corresponding Author

*E-mail: daniel.lienhard@env.ethz.ch.

Notes

The authors declare no competing financial interest.

ACKNOWLEDGMENTS

This work was supported by the ETH Research Grant ETH-0210-1. J.P.R. and D.L.B. acknowledge the EPSRC for financial support through the award of a leadership fellowship to J.P.R..

REFERENCES

(1) Seinfeld, J. H.; Pandis, S. N. *Atmospheric Chemistry and Physics*; Wiley and Sons Inc.: New York, 1998.
(2) Goldstein, A. H.; Galbally, I. E. *Environ. Sci. Technol.* **2007**, *41*, 1514−1521.
(3) Zhang, Q.; Jimenez, Z. L.; Canagaratna, M. L.; Allan, J. D.; Coe, H.; Ulbrich, I.; Alfarra, M. R.; Takami, A.; Middlebrook, A. M.; Sun, Y. L.; et al. *Geophys. Res. Lett.* **2007**, *34*, L13801.
(4) Peng, C. G.; Chan, M. N.; Chan, C. K. *Environ. Sci. Technol.* **2001**, *35*, 4495−4501.
(5) Peng, C. G.; Chow, A. H. L.; Chan, C. K. *Aerosol Sci. Technol.* **2001**, *35*, 753−758.
(6) Chan, M. N.; Choi, M. Y.; Ng, N. L.; Chan, C. K. *Environ. Sci. Technol.* **2005**, *39*, 1555−1562.
(7) Zuend, A.; Marcolli, C.; Booth, A. M.; Lienhard, D. M.; Soonsin, V.; Krieger, U. K.; Top-ping, D. O.; McFiggans, G.; Peter, T.; Seinfeld, J. H. *Atmos. Chem. Phys.* **2011**, *11*, 9155−9206.
(8) Wilson, T. W.; Murray, B. J.; Wagner, R.; Möhler, O.; Saathoff, H.; Schnaiter, M.; Skrotzki, J.; Price, H. C.; Malkin, T. L.; Dobbie, S.; et al. *Atmos. Chem. Phys.* **2012**, *12*, 8611−8632.
(9) Karrer, P.; Smirnoff, A. P. *Helv. Chim. Acta* **1921**, *4*, 817−820.
(10) Peat, S. *Adv. Carbohydr. Chem.* **1946**, *2*, 37−78.
(11) Shafizadeh, F.; Furneauf, R. H.; Cochran, T. G.; Scholl, J. P.; Sakai, Y. *J. Appl. Polym. Sci.* **1979**, *23*, 3525−3539.
(12) Schauer, J. J.; Kleeman, M. J.; Cass, G. R.; Simoneit, B. R. T. *Environ. Sci. Technol.* **2001**, *35*, 1716−1728.
(13) Fine, P. M.; Cass, G. R.; Simoneit, B. R. T. *Environ. Sci. Technol.* **2001**, *35*, 2665−2675.
(14) Jordan, T. B.; Seen, A. J. *Environ. Sci. Technol.* **2005**, *39*, 3601−3610.
(15) Decesari, S.; Fuzzi, S.; Facchini, M. C.; Mircea, M.; Emblico, L.; Cavalli, F.; Maenhaut, W.; Chi, X.; Schkolnik, G.; Falkovich, A.; et al. *Atmos. Chem. Phys.* **2006**, *6*, 375−402.
(16) Simoneit, B. R. T.; Schauer, J. J.; Nolte, C. G.; Oros, D. R.; Elias, V. O.; Fraser, M. P.; Rogge, W. F.; Cass, G. R. *Atmos. Environ.* **1999**, *33*, 173−182.
(17) Epstein, Y. V.; Maksimenko, N. S.; Fedorchenko, R. I. *Latv. PSR Zinat. Akad. Vestis Kim. Ser.* **1967**, 119−121.
(18) Zamora, I. R.; Tabazadeh, A.; Golden, D. M.; Jacobson, M. Z. *J. Geophys. Res.* **2011**, *116*, D23207.
(19) Graham, B.; Mayol-Bracero, O. L.; Guyon, P.; Roberts, G. C.; Decesari, S.; Facchini, M. C.; Artaxo, P.; Maenhaut, W.; Koll, P.; Andreae, M. O. *J. Geophys. Res.* **2002**, *107*, 8047.
(20) Jung, J.; Kawamura, K. *Atmos. Environ.* **2011**, *45*, 5266−5272.
(21) Murray, B. J. *Atmos. Chem. Phys.* **2008**, *8*, 5423−5433.
(22) Murray, B. J.; Wilson, T. W.; Dobbie, S.; Cui, Z.; Al-Jumur, S. M. R. K.; Möhler, O.; Schnaiter, M.; Wagner, R.; Benz, S.; Niemand, M.; et al. *Nat. Geosci.* **2010**, *3*, 233−237.
(23) White, J. C. D.; Davies, D. T. *J. Dairy Res.* **1963**, *30*, 171.
(24) Fulcrand, H.; Cheynier, V.; Oszmianski, J.; Moutounet, M. *Phytochemistry* **1997**, *46*, 223−227.
(25) Maltini, E.; Anese, M.; Shtylla, I. *Cryoletters* **1997**, *18*, 263−268.
(26) Tang, I. N.; Munkelwitz, H. R. *Aerosol Sci. Technol.* **1991**, *15*, 201−207.
(27) Tang, I. N.; Munkelwitz, H. R. *J. Geophys. Res.* **1994**, *99*, 18801−18808.
(28) Tang, I. N. *J. Geophys. Res.* **1996**, *101*, 19245−19250.
(29) Usher, C. R.; Michel, A. E.; Grassian, V. H. *Chem. Rev.* **2003**, *103*, 4883−4939.
(30) Zuend, A.; Marcolli, C.; Luo, B. P.; Peter, T. *Atmos. Chem. Phys.* **2008**, *8*, 4559−4593.
(31) Fredenslund, A.; Jones, R. L.; Prausnitz, J. M. *AIChE J.* **1975**, *21*, 1086−1099.
(32) Hansen, H. K.; Rasmussen, P.; Fredenslund, A.; Schiller, M.; Gmehling, J. *Ind. Eng. Chem. Res.* **1991**, *30*, 2352−2355.
(33) Zdanovskii, A. B. *Tr. Solyanoi Lab. Akad. Nauk SSSR* **1936**, 5−70.
(34) Zdanovskii, A. B. *Zh. Fiz. Khim.* **1948**, *22*, 1478−1485.
(35) Stokes, R. H.; Robinson, R. A. *J. Phys. Chem.* **1966**, *70*, 2126.
(36) Zobrist, B.; Marcolli, C.; Koop, T.; Luo, B. P.; Murphy, D. M.; Lohmann, U.; Zardini, A. A.; Krieger, U. K.; Corti, T.; Cziczo, D. J.; et al. *Atmos. Chem. Phys.* **2006**, *6*, 3115−3129.
(37) Zobrist, B.; Marcolli, C.; Pedernera, D. A.; Koop, T. *Atmos. Chem. Phys.* **2008**, *8*, 5221−5244.
(38) Zobrist, B.; Soonsin, V.; Luo, B. P.; Krieger, U. K.; Marcolli, C.; Peter, T.; Koop, T. *Phys. Chem. Chem. Phys.* **2011**, *13*, 3514−3526.
(39) Mitchem, L.; Hopkins, R. J.; Buajarern, J.; Ward, A. D.; Reid, J. P. *Chem. Phys. Lett.* **2006**, *432*, 362−366.
(40) Mitchem, L.; Reid, J. P. *Chem. Soc. Rev.* **2008**, *37*, 756−769.
(41) Wills, J. B.; Knox, K. J.; Reid, J. P. *Chem. Phys. Lett.* **2009**, *481*, 153−165.
(42) Hargreaves, G.; Kwamena, N. O. A.; Zhang, Y. H.; Butler, J. R.; Rushworth, S.; Clegg, S. L.; Reid, J. P. *J. Phys. Chem. A* **2010**, *114*, 1806−1815.
(43) Miles, R. E. H.; Guillon, M.; Mitchem, L.; McGloin, D.; Reid, J. P. *Phys. Chem. Chem. Phys.* **2009**, *11*, 7312−7317.
(44) Miles, R. E. H.; Walker, J. S.; Burnham, D. R.; Reid, J. P. *Phys. Chem. Chem. Phys.* **2012**, *14*, 3037−3047.
(45) Braun, C.; Krieger, U. K. *Opt. Express* **2001**, *8*, 314−321.
(46) Zardini, A. A.; Krieger, U. K.; Marcolli, C. *Opt. Express* **2006**, *14*, 6951−6962.
(47) Angell, C. A. *Chem. Rev.* **2002**, *102*, 2627−2649.
(48) Marcolli, C.; Gedamke, S.; Peter, T.; Zobrist, B. *Atmos. Chem. Phys.* **2007**, *7*, 5081−5091.

(49) Corti, H. R.; Angell, C. A.; Auffret, T.; Levine, H.; Pilar Buera, M.; Reid, D. S.; Roos, Y. H.; Slade, L. *Pure Appl. Chem.* **2010**, *82*, 1065−1097.
(50) Pedernera, D. A. Ph.D. Thesis, University of Bielefeld, 2008.
(51) Kadoya, S.; Izutsu, K. I.; Yonemochi, E.; Terada, K.; Yomota, C.; Kawanishi, T. *Chem. Pharm. Bull.* **2008**, *56*, 821−826.
(52) Izutsu, K.; Kadoya, S.; Yomota, C.; Kawanishi, T.; Yonemochi, E.; Terada, K. *Chem. Pharm. Bull.* **2009**, *57*, 43−48.
(53) Fukuoka, E.; Makita, M.; Yamamura, S. *Chem. Pharm. Bull.* **1989**, *37*, 1047−1050.
(54) Kendall, J.; Booge, J. E.; Andrews, J. C. *J. Am. Chem. Soc.* **1917**, *39*, 2303−2323.
(55) Hall, R. E.; Sherrill, M. S. Freezing-point lowerings of aqueous solutions. In *International Critical Tables*; McGraw-Hill Book Company: New York, 1930.
(56) Apelblat, A.; Manzurola, E. *J. Mol. Liq.* **2003**, *103*, 201−210.
(57) Shafizadeh, F.; McGinnis, G. D.; Philpo, C. W.; Susott, R. A. *Carbohydr. Res.* **1970**, *13*, 184.
(58) Smith, G. W.; Shafizadeh, F. *J. Chem. Soc. B* **1971**, 908−911.
(59) Hosoya, T.; Kawamoto, H.; Saka, S. *J. Anal. Appl. Pyrolysis* **2008**, *83*, 64−70.
(60) Descamps, M.; Correia, N. T.; Derollez, P.; Danede, F.; Capet, F. *J. Phys. Chem. B* **2005**, *109*, 16092−16098.
(61) Benkhof, S.; Kudlik, A.; Blochowicz, T.; Rossler, E. *J. Phys.: Condens. Matter* **1998**, *10*, 8155−8171.
(62) Brand, R.; Lunkenheimer, P.; Loidl, A. *J. Chem. Phys.* **2002**, *116*, 10386−10401.
(63) Kabtoul, B.; Ramos, M. A. *Phys. Status Solidi A* **2011**, *208*, 2249−2253.
(64) Haida, O.; Suga, H.; Seki, S. *J. Chem. Thermodynamics* **1977**, *9*, 1133−1148.
(65) Haida, O.; Suga, H.; Seki, S. *Bull. Chem. Soc. Jpn.* **1977**, *50*, 802−809.
(66) Murthy, S. S. N. *Thermochim. Acta* **2000**, *359*, 143−159.
(67) Ramos, M. A.; Shmytko, I. M.; Arnautova, E. A.; Jimenez-Rioboo, R. J.; Rodriguez-Mora, V.; Vieira, S.; Capitan, M. J. *J. Non-Cryst. Solids* **2006**, *352*, 4769−4775.
(68) Angell, C. A.; Sare, J. M.; Sare, E. J. *J. Phys. Chem.* **1978**, *82*, 2622−2629.
(69) Gordon, J. M.; Taylor, J. S. *J. Appl. Chem.* **1952**, *2*, 493−500.
(70) Johari, G. P.; Hallbrucker, A.; Mayer, E. *Nature* **1987**, *330*, 552−553.
(71) Johari, G. P. *J. Chem. Phys.* **2002**, *116*, 8067−8073.
(72) Kohl, I.; Bachmann, L.; Hallbrucker, A.; Mayer, E.; Loerting, T. *Phys. Chem. Chem. Phys.* **2005**, *7*, 3210−3220.
(73) Murphy, D. M.; Koop, T. *Q. J. R. Meteorol. Soc.* **2005**, *131*, 1539−1565.
(74) Koop, T.; Luo, B. P.; Tsias, A.; Peter, T. *Nature* **2000**, *406*, 611−614.
(75) Koop, T.; Zobrist, B. *Phys. Chem. Chem. Phys.* **2009**, *11*, 10839−10850.
(76) Lightstone, J. M.; Onasch, T. B.; Imre, D.; Oatis, S. *J. Phys. Chem. A* **2000**, *104*, 9337−9346.
(77) Zardini, A. A.; Krieger, U. K. *Opt. Express* **2009**, *17*, 4659−4669.
(78) Clegg, S. L.; Brimblecombe, P.; Wexler, A. S. *J. Phys. Chem. A* **1998**, *102*, 2137−2154.
(79) Koop, T.; Bookhold, J.; Shiraiwa, M.; Pöschl, U. *Phys. Chem. Chem. Phys.* **2011**, *13*, 19238−19255.
(80) Tong, H.-J.; Reid, J. P.; Bones, D. L.; Luo, B. P.; Krieger, U. K. *Atmos. Chem. Phys.* **2011**, *11*, 4739−4754.
(81) Bones, D. L.; Reid, J. P.; Lienhard, D. M.; Krieger, U. K. *Proc. Natl. Acad. Sci. U.S.A.* **2012**, *109*, 11613−11618.
(82) Laguerie, C.; Aubry, M.; Couderc, J. P. *J. Chem. Eng. Data* **1976**, *21*, 85−87.
(83) Kharat, S. J. *Int. J. Appl. Chem.* **2008**, *4*, 223−235.
(84) Haynes, W. M. Physical Constants of Organic Compounds. In *CRC Handbook of Chemistry and Physics*, 91st ed. (internet version); CRC Press/Taylor and Francis: Boca Raton, FL, 2011.
(85) Pitzer, K. S. *Thermodynamics*; McGraw-Hill, Inc.: New York, 1995.
(86) Clegg, S. L.; Wexler, A. S. *J. Phys. Chem. A* **2011**, *115*, 3393−3460.
(87) Clegg, S. L.; Wexler, A. S. *J. Phys. Chem. A* **2011**, *115*, 3461−3474.
(88) Moelwyn-Hughes, E. A. *Physical Chemistry*, 2nd rev. ed.; Pergamon: New York, 1961; p 397.
(89) Born, M.; Wolf, E. *Principles of Optics*; Cambridge University Press: New York, 1999.
(90) Pickard, R. H.; Houssa, A. H. J.; Hunter, H. Refractivity of mixtures. In *International Critical Tables*; McGraw-Hill Book Company: New York, 1930.
(91) Stolle, R. *Z. Ver. Dtsch. Zucker Ind.* **1901**, *51*, 469−487.
(92) Zerban, F. W.; Martin, J. *J. AOAC Int.* **1951**, *34*, 808−812.
(93) Crenshaw, J. L. Densities (specific gravitites) and thermal expansion of aqueous solutions of organic compounds. In *International Critical Tables*; McGraw-Hill Book Company: New York, 1930.
(94) Levien, B. J. *J. Phys. Chem.* **1955**, *59*, 640−644.
(95) Manzurola, E.; Apelblat, A. *J. Chem. Thermodyn.* **1985**, *17*, 579−584.
(96) Apelblat, A.; Manzurola, E. *Fluid Phase Equilib.* **1990**, *60*, 157−171.
(97) Kharat, S. J. *Int. J. Thermophys.* **2010**, *31*, 585−594.
(98) Dunlop, P. J. *J. Phys. Chem.* **1956**, *60*, 1464−1465.
(99) Banipal, P. K.; Banipal, T. S.; Lark, B. S.; Ahluwalia, J. C. *J. Chem. Soc., Faraday Trans.* **1997**, *93*, 81−87.
(100) Banipal, P. K.; Chahal, A. K.; Banipal, T. S. *J. Chem. Thermodyn.* **2009**, *41*, 452−483.
(101) Blanco, P.; Kriegs, H.; Arlt, B.; Wiegand, S. *J. Phys. Chem. B* **2010**, *114*, 10740−10747.
(102) Armstrong, D. M. G. *Discuss. Faraday Soc.* **1954**, 45−58.
(103) Slade, L.; Levine, H. *Pure Appl. Chem.* **1988**, *60*, 1841−1864.
(104) Levine, H.; Slade, L. *J. Chem. Soc., Faraday Trans.* **1988**, *84*, 2619−2633.
(105) Lienhard, D. M.; Zobrist, B.; Zuend, A.; Krieger, U. K.; Peter, T. *J. Chem. Phys.* **2012**, *136*, 074515.
(106) Park, Y. J.; Kim, H. S.; Jeffrey, G. A. *Acta Crystallogr., Sect. A* **1969**, *A 25*, S197.
(107) Apelblat, A.; Dov, M.; Wisniak, J.; Zabicky, J. *J. Chem. Thermodyn.* **1995**, *27*, 35−41.
(108) Velezmoro, C. E.; Meirelles, A. J. A. *Drying Technol.* **1998**, *16*, 1789−1805.
(109) Maffia, M. C.; Meirelles, A. J. A. *J. Chem. Eng. Data* **2001**, *46*, 582−587.
(110) Knopf, D. A.; Lopez, M. D. *Phys. Chem. Chem. Phys.* **2009**, *11*, 8056−8068.
(111) Knopf, D. A.; Rigg, Y. J. *J. Phys. Chem. A* **2011**, *115*, 762−773.
(112) Paterno, E.; Cingolani, M. *Kolloid Z.* **1914**, *14*, 74−81.